Materials Advances

ROYAL SOCIETY OF CHEMISTRY

PAPER

View Article Online
View Journal | View Issue

Cite this: *Mater. Adv.*, 2022, 3, 7966

Combining gellan gum with a functional low-molecular-weight gelator to assemble stiff shaped hybrid hydrogels for stem cell growth†

Carmen C. Piras, [a] Paul G. Genever[b] and David K. Smith *[a]

We report hybrid hydrogels that combine gellan gum (GG) polymer gelator (PG) with a low-molecular weight gelator (LMWG) based on 1,3:2,4-dibenzylidene sorbitol (DBS). We fabricate these gels into beads using a heat–cool cycle to set the LMWG gel and then using different calcium sources ($CaCl_2$ and $CaCO_3$) to subsequently crosslink the gellan gum. In the case of $CaCO_3$, glucono-δ-lactone (GdL) is used as a slow acidification agent to slowly solubilise calcium ions and induce GG crosslinking. Alternatively the photoacid generator, diphenyliodonium nitrate (DPIN) can be used with UV irradiation to solubilise $CaCO_3$ and induce GG gelation, in which case, a photomask applied to gels made in trays yields photopatterned gels. Combining the LMWG with gellan gum further enhances the stiffness of GG, and importantly, makes the gels significantly more resistant to shear strain. LMWG/GG hybrid gels are considerably stiffer than equivalent LMWG/alginate gels. The DBS-$CONHNH_2$ LMWG retains its unique ability to reduce precious metal salts to nanoparticles (NPs) within the hybrid gel beads, as demonstrated by the *in situ* fabrication of AgNPs. The hybrid gel beads support the growth of human mesenchymal stem cells for extended periods of time. We suggest that the favourable rheological properties of these hybrid gels, combined with the ability of the LMWG to form AgNPs *in situ*, may enable potential future orthopedic applications.

Received 20th May 2022,
Accepted 22nd August 2022

DOI: 10.1039/d2ma00565d

rsc.li/materials-advances

Introduction

Gels are fascinating soft materials, intermediate between solids and liquids, with wide-ranging applications from food technology and personal care through to drug delivery and regenerative medicine.[1] Gels can be formed by a variety of different systems – particularly important amongst these are gels formed by polymer gelators (PGs)[2] and those formed by low-molecular-weight gelators (LMWGs).[3] Each of these classes of gelator offers specific advantages, and in recent years, combining the two to yield hybrid hydrogels has emerged as a powerful strategy for creating addressable, tunable multi-component soft materials.[4] This can provide access to shaped and patterned gel-phase materials with high added value.[5] With this strategy in mind, we became interested in the use of gellan gum as the polymeric component of such hybrid gels.

Gellan gum is a low-cost extracellular polysaccharide produced by *Sphingomonas* bacteria.[6] This anionic polymer is typically composed of tetrasaccharide repeat units consisting of two D-glucose, one D-glucuronic acid and one L-rhamnose residues (*i.e.* [D-Glc(β1 → 4)D-GlcA(β1 → 4)D-Glc(β1 → 4)L-Rha(α1 → 3)]*n*, Fig. 1). Gellan gum is mainly used as a gelling agent, and is typically activated either thermally or by cross-linking with divalent metal cations. Having only been

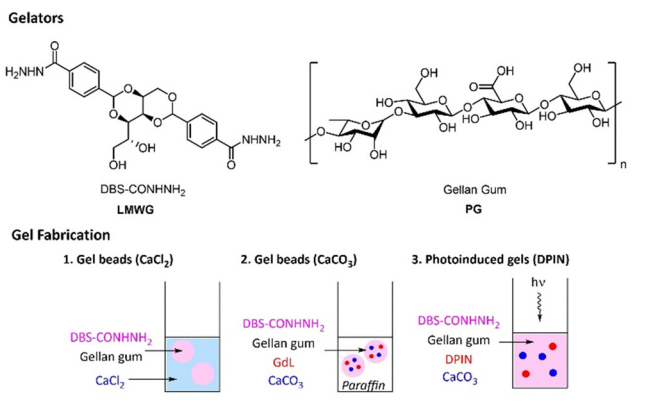

Fig. 1 Chemical structures of DBS-$CONHNH_2$ and gellan gum, and schematic methods of fabrication of hybrid gels: (1) gel beads using $CaCl_2$, (2) gel beads using $CaCO_3$ and glucono-δ-lactone (GdL), and (3) photo-induced gels using $CaCO_3$ and diphenyliodonium nitrate (DPIN).

[a] *Department of Chemistry, University of York, Heslington, York, YO10 5DD, UK. E-mail: david.smith@york.ac.uk*
[b] *Department of Biology, University of York, Heslington, York, YO10 5NG, UK*

† Electronic supplementary information (ESI) available: Full details of gel fabrication methods and characterisation data, biological assay methods and additional data. See DOI: https://doi.org/10.1039/d2ma00565d

discovered in 1978, and FDA approved in 1992,[7] it is a relatively 'young' biomaterial compared to other gelling polysaccharides, such as agarose, alginate or cellulose. However, thanks to its ease of gelation, tuneable physical properties and versatility, research on this PG has seen significant recent expansion. In the food industry, it is widely used as a thickener, stabilizer and binder, as well as a replacement for gelatine in vegan products.[8] Biomedical applications of gellan gum hydrogels include, tissue engineering, repair and regeneration,[9] biosensor synthesis[10] and pharmaceutical formulation for oral, nasal, topical and injectable administration.[11] However, gellan gum has some disadvantages in terms of its use in regenerative medicine – specifically its relatively brittle nature and a lack of attachment sites for anchorage-dependent cells.[12] As such, making synthetic modifications to gellan gum and/or blending it with a different additives has become an area of significant interest.[13]

Research in our group has recently explored multicomponent hybrid hydrogels based on calcium alginate and the low molecular weight gelators (LMWGs) based on 1,3:2,4-dibenzylidene sorbitol (DBS), *i.e.* DBS-CONHNH$_2$ and DBS-COOH (Fig. 1).[14] We have demonstrated that in such hybrid gels, the LMWGs provided functionality, whilst the alginate offered mechanical support and robustness to shape and structure the LMWGs into gel beads or tubes. On starting this work with gellan gum, we wanted to explore the potential use of this PG instead of calcium alginate to develop gels with enhanced properties. Taking into account the wide range of applications of gellan gum, we reasoned that this polymer could be an interesting alternative to alginate for the formulation of LMWG/PG hybrid gels. In particular, the high stiffness of gellan gum was attractive as it may broaden the rheological range over which our LMWGs can operate, potentially opening up new applications.

We thus report the fabrication of shaped and patterned hybrid gels comprising DBS-CONHNH$_2$ and gellan gum (GG), exploring how their rheological properties combine in a synergistic way. The LMWG retains its unique feature of inducing *in situ* formation of silver nanoparticles (AgNPs),[15] and the resulting hybrid hydrogels are compatible with the growth of human mesenchymal stem cells. We suggest such materials may have potential future uses in regenerative medicine.

Results and discussion

Hybrid DBS-CONHNH$_2$/GG gel beads cross-linked with CaCl$_2$

DBS-CONHNH$_2$ was synthesized in good yield by our previously reported procedure.[16] This LMWG forms hydrogels by a heat–cool cycle. Gellan gum (GG) is a commercially-available polysaccharide and was used as supplied (Alfa Aesar). GG can form stiff hydrogels when cross-linked with Ca^{2+} ions. Therefore, the LMWG was used as a scaffold to support the subsequent gelation of GG, induced by Ca^{2+}.

Initially DBS-CONHNH$_2$/GG gel beads were prepared by the emulsion method previously described by us,[14] with CaCl$_2$ being used for crosslinking (Fig. 1). Briefly, DBS-CONHNH$_2$ (0.3% wt/vol) was suspended in water (0.5 mL) and then combined with an aqueous GG solution (0.1–1.0% wt/vol, 0.5 mL). The suspension was heated until complete dissolution of the solid particles and subsequently added dropwise (20 μL per drop) to paraffin oil (40 mL). The droplets were left undisturbed for 20 min to allow assembly of the DBS-CONHNH$_2$ network, which acts as a scaffold to support the subsequent gelation of GG. To cross-link GG, the gel beads were then transferred to a CaCl$_2$ solution (5.0% wt/vol) and gently mixed for *ca.* 20 min to allow diffusion of the Ca^{2+} into them. After this time, to remove residual paraffin oil, the gel beads were washed with petroleum ether, then EtOH and finally water. Small beads with a 3.0–3.5 mm diameter were obtained (Fig. 2a). The bead diameter is controlled by the droplet size during fabrication – smaller gel beads could be obtained by addition of smaller volumes.[14a,e]

In this method, the Ca^{2+} ions are readily available and quickly cross-link the polymer from the outside, then penetrate inside the gel beads by diffusion. Possibly as a result of this, the surface and cross-section of the beads appear heavily wrinkled (Fig. 2b and c). Optical microscopy of the gel bead cross-section, embedded into resin and stained with toluidine blue, showed a uniform distribution of gel networks, consistent with a model in which they are woven within the gel beads (Fig. 2d). SEM microscopy of the gel beads showed a wrinkled surface and a nanofibrillar core, thus further confirming the incorporated gelators were in their self-assembled state (Fig. 2e, f and Fig. S7, ESI†), although it was not possible to distinguish the two networks using this approach. TEM images were also recorded (Fig. S4–S6, ESI†).

To confirm the two gelators were self-assembled within the gel beads, we recorded a standard ^{1}H NMR spectrum of five gel beads in D_2O, in the presence of DMSO (1.4 μL) as internal standard. The lack of any signals in the recorded spectra indicates that both gelators are completely 'immobilised' within the gel beads (Fig. S1, ESI†).

Another simple ^{1}H NMR spectroscopy experiment, carried out on 10 dried beads, subsequently dissolved in DMSO-d$_6$ in

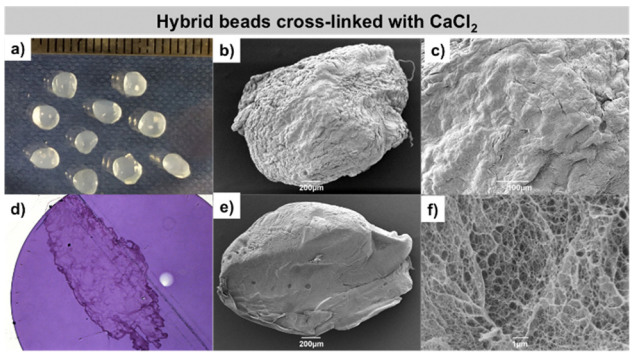

Fig. 2 Images of DBS-CONHNH$_2$/GG hybrid gel beads cross-linked with CaCl$_2$. (a) Photographic images of the gel beads. (b and c) SEM images of a whole gel bead and gel bead surface. (d) Optical microscopy of gel bead cross-section embedded into resin and stained with toluidine blue. (e and f) SEM images of gel bead cross-section. *N.B.* image (d): the gel bead section was fragmented during preparation.

the presence of an internal standard (MeCN), allowed estimation of the amount of LMWG incorporated into each bead. By comparing the aromatic C–H integrals of DBS-$CONHNH_2$ with the internal standard we could quantify how much LMWG had been incorporated into the beads. Given the beads were prepared using 20 μL per droplet, in theory, 1 mL can prepare 50 beads. Since an initial 0.3% wt/vol concentration of DBS-$CONHNH_2$ was used, corresponding to 6.32 μmol, each gel bead can contain up to 0.126 μmol of LMWG. Our study indicated that each hybrid bead incorporates *ca.* 0.11 μmol of DBS-$CONHNH_2$ (Fig. S2, ESI†). Therefore, the vast majority of the LMWG initially loaded is retained inside the gel beads.

The macroscopic physical properties of the gels were then studied in terms of thermal stability and rheological behaviour. Initially, the thermal stability of equivalent gels made in sample vials was evaluated using a simple tube-inversion method. The gel–sol transition temperature of DBS-$CONHNH_2$ (0.4% wt/vol) is 86 °C. In the presence of increasing GG loadings (0.1, 0.3, 0.5 and 1.0% wt/vol), this rises to >100 °C (Table S1, ESI†). As expected therefore, the PG improves the thermal stability.

To study the thermal stability of the hybrid gel beads in more detail over time, we performed an NMR experiment at 90 °C and monitored the disassembly of the LMWG, as the LMWG becomes mobile, its ^{1}H NMR resonances increase in intensity. After only 15 min *ca.* 40% of the LMWG had disassembled, increasing to a maximum of *ca.* 60% after 3.5 h (Table S3, ESI†). It is possible that not all LMWG is mobilised since $CaCl_2$ cross-links GG by diffusion from the outside of the beads, a tougher GG 'shell' could form, somewhat protecting the LMWG network from being thermally disrupted and dissolved into the hot solvent.

Importantly, the mechanical properties of the hybrid gels were then studied by oscillatory rheology (Table 1). To record reproducible parallel plate rheometry data it was necessary to use equivalent gel discs made in sample tubes, rather than testing the beads (see ESI†). The DBS-$CONHNH_2$ gel has an elastic modulus (G') of *ca.* 800 Pa (Fig. S9, ESI†), which increases to 3980, 11 200, 23 500 and 46 600 with increasing GG loadings (0.1, 0.3, 0.5, 1.0% wt/vol) – a remarkable increase in stiffness. To some extent, this was partly expected, as GG is a stiff gel,[17] however, the values obtained are even higher than those of the G' values of the GG gels alone (3290, 4560, 10 500 and 17 300 Pa; respectively at 0.4, 0.6, 0.8 and 1.3% wt/vol concentrations; Fig. S10–S13, ESI†). This suggests that the inter-penetrating PG/LMWG networks within the hybrid material significantly stiffen the gel.

Furthermore, it is informative to consider the shear strain at which the gels break down as defined by the G'/G'' crossover points. On its own, gellan gum, although a stiff gel, has very poor resistance to shear, and is brittle, fracturing easily. Indeed, this is a significant drawback in terms of its use in some applications.[12] Indeed, we found that for GG alone, $G' = G''$ at a shear strain of only *ca.* 1%. However, on blending with DBS-$CONHNH_2$, the stability to shear strain increases significantly – up to 7.7% for the sample containing 0.3% wt/vol DBS-$CONHNH_2$ and 0.3% wt/vol GG. The high shear resistance of DBS-$CONHNH_2$ (*ca.* 25% shear strain) therefore translates into these hybrid gels and very significantly improves the rheological operating window of GG.

Table 1 Rheological data as determined using oscillatory rheometry with a parallel plate geometry, for DBS-$CONHNH_2$ gels, gellan gum gels, alginate gels and hybrid gels based on gellan gum/LMWG or alginate/LMWG.[14a] In all cases, the PG component is crosslinked using 5% wt/vol $CaCl_2$. Loadings are given in % wt/vol. G' values are given in Pa. The G'/G'' crossover point refers to the % shear strain at which $G'' = G'$

LMWG load (%)	GG load (%)	Alginate load (%)	Total load (%)	Gel trigger	G' (Pa)	G'/G'' crossover (%)
0.4	—	—	0.4	Heat/cool	800	25.1
—	0.4	—	0.4	$CaCl_2$	3290	1.0
—	0.6	—	0.6	$CaCl_2$	4560	1.1
—	0.8	—	0.8	$CaCl_2$	10 500	2.0
—	1.3	—	1.3	$CaCl_2$	17 300	1.0
0.3	0.1	—	0.4	$CaCl_2$	3980	6.3
0.3	0.3	—	0.6	$CaCl_2$	11 200	7.7
0.3	0.5	—	0.8	$CaCl_2$	23 500	6.9
0.3	1.0	—	1.3	$CaCl_2$	46 600	2.3
—	—	0.4	0.4	$CaCl_2$	490	6.5
—	—	0.6	0.6	$CaCl_2$	1420	19.9
—	—	0.8	0.8	$CaCl_2$	2500	2.3
—	—	1.3	1.3	$CaCl_2$	17 100	8.5
0.3	—	0.1	0.4	$CaCl_2$	1730	50.6
0.3	—	0.3	0.6	$CaCl_2$	6030	41.2
0.3	—	0.5	0.8	$CaCl_2$	8030	18.4
0.3	—	1.0	1.3	$CaCl_2$	17 500	2.8

It is worth comparing the performance of these GG/LMWG hybrid gels with the alginate/LMWG hybrid gels previously reported by us.[14a] As might be expected, the GG/LMWG hybrids are very significantly stiffer than those based on alginate. Indeed, with G' values up to *ca.* 50 kPa, gellan gum moves these hybrids into the range of stiffnesses required for effective osteogenesis (*i.e.*, differentiation of stem cells into bone cells).[17] At the same time, the LMWG makes the GG significantly more resistant to shear strain than native GG, improving its handling. Furthermore, it adds additional function to the gels that may be useful in an osteogenesis setting (see below).

In summary therefore, GG provides DBS-$CONHNH_2$ with stiffness, while DBS-$CONHNH_2$ provides GG with greater shear resistance, meaning that these hybrid hydrogels may extend the potential applications of both LMWG and PG by combining the best of their individual rheological characteristics.

Hybrid DBS-$CONHNH_2$/GG gel beads cross-linked with $CaCO_3$/GdL

A different procedure was then applied to obtain DBS-$CONHNH_2$/GG gel beads using $CaCO_3$ as a cross-linker. $CaCO_3$ is insoluble in water, and therefore cannot directly crosslink gellan gum. However it has been shown for other polysaccharides that on slow acidification, Ca^{2+} is released and gel crosslinking can take place.[18] To achieve slow acidification, gluconо-δ-lactone (GdL) is ideal – it slowly hydrolyses, and lowers pH over a period of hours.[19] This approach has previously been quite extensively used to crosslink alginate hydrogels.[20] GdL has also been combined with calcium carbonate to form alginate/GG hybrids, although it is not clear whether the gellan

gum was actually crosslinked *via* the same mechanism as the alginate in this case.[21] There has been some interest in incorporating $CaCO_3$ microparticles into GG gels – they can slowly release Ca^{2+} even in the absence of an acid source and are also highly relevant in bone tissue engineering.[22] GdL alone has also been used to trigger the assembly of emulsion gels based on GG,[23] which can be achieved if the pH drops below 3.5. As far as we can tell, however, although widely used for alginate gels, it has not been clearly demonstrated that the $CaCO_3$/GdL approach can crosslink gellan gum *via* Ca^{2+} release, and we therefore wanted to test this. We found that GG gels in vials could be produced using this approach (see ESI† and characterisation below).

We therefore moved on to test this approach for making hybrid gel beads, in the same way we had previously reported for alginate/LMWG hybrids.[14d] After dropwise addition of the hot mixture containing the two gelators, GdL and $CaCO_3$ into paraffin oil, the droplets were left undisturbed overnight to allow the slow release of Ca^{2+} ions that cross-link GG *in situ* (Fig. 1). After this time, small gel beads (diameter 3.0–3.5 mm) were collected from paraffin oil and washed multiple times as described above (Fig. 3a). The final pH of the gel beads is 5–6, with the precise value depending on the amount of GdL used in the formation process (Fig. S18 and S19, ESI†). As such, we are confident that the GdL is not inducing GG assembly simply by protonation of the polymer backbone itself, as that would require the pH to fall significantly lower.[23]

Although this method of bead formation is similar to that using $CaCl_2$, in this case, the release of Ca^{2+} takes place slowly over time, throughout the bead itself, rather than rapidly from the periphery. As such, GG gelation happens in a more homogeneous, temporally-controlled manner. This leads to more uniform gel beads with smoother surfaces (Fig. 3b, c and Fig. S26, ESI†). Furthermore, because the beads are formed in paraffin, they are more uniform and spherical (Fig. 3a) than the beads crosslinked with $CaCl_2$ (Fig. 2a). Optical microscopy of the gel bead cross-section, embedded into resin and stained with toluidine blue, showed a uniform distribution of the two gel networks, consistent with a model in which they are woven within the gel beads (Fig. 3c and Fig. S23, ESI†). SEM microscopy showed a nanofibrillar gel bead core, thus further confirming that the incorporated gelators were in their self-assembled state (Fig. 3e, f and Fig. S27, ESI†). The data were consistent with assembly of both gelators, although unfortunately did not allow us to distinguish between the self-assembled networks formed by the individual components. TEM images of the different gels were also recorded (Fig. S24 and S25, ESI†).

Once again, ^{1}H NMR spectroscopy was used to confirm that the two gelators were self-assembled within the gel beads, with data indicating both gelators are completely 'immobilised' (Fig. S20, ESI†). Using NMR to estimate the amount of LMWG incorporated into each bead (see method above), we found that each $CaCO_3$ hybrid bead incorporates *ca.* 0.10 μmol (Fig. S21, ESI†) of the theoretical maximum of 0.126 μmol – *ca.* 80%. Therefore, the majority of the LMWG is retained inside the gel beads.

Like the gels formed using $CaCl_2$, the thermal stability of the hybrid gels triggered by $CaCO_3$/GdL gels is >100 °C (0.15% wt/vol $CaCO_3$/1.0% wt/vol GdL; Table S4, ESI†) as measured by tube inversion, with the PG improving the thermal stability of the gel. More detailed NMR studies indicated that when the gel beads were incubated at 90 °C, after only 15 min *ca.* 40% of the LMWG was disassembled (Table S3, ESI†), increasing to a maximum of *ca.* 71% after 5.5 h. This is broadly similar to the $CaCl_2$ system – the slightly greater degree of LMWG disassembly may reflect the fact that for the $CaCO_3$/GdL gel beads the exterior is less heavily crosslinked GG.

The mechanical properties of these hybrid gels were then studied by oscillatory rheology using gel discs (Table 2 and Table. S5, ESI†). As for the gels triggered by $CaCl_2$, the presence of gellan gum increased the stiffness of the gel very significantly, with G' values of 2580, 11 300 and 19 300 Pa with increasing GG loadings (0.1, 0.3 and 0.5% wt/vol; Fig. S33–S35, ESI†); once again, these were higher than the G' values of GG-only gels (1760, 4630 and 8950 Pa; Fig. S30–S32, ESI†) demonstrating the benefits of interpenetrated LMWG/PG networks. Once again, these stiffnesses are higher than those previously reported for equivalent alginate/LMWG hybrid hydrogels (data not shown).[14d]

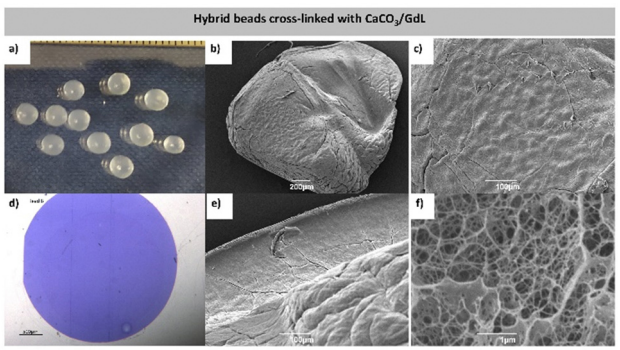

Fig. 3 Images of DBS-$CONHNH_2$/GG hybrid gel beads cross-linked with $CaCO_3$/GdL. (a) Photographic images of the gel beads. (b and c) SEM images of a whole gel bead and gel bead surface. (d) Optical microscopy of gel bead cross-section embedded into resin and stained with toluidine blue. (e and f) SEM images of gel bead cross-section.

Table 2 Rheological data as determined using oscillatory rheometry with a parallel plate geometry, for DBS-$CONHNH_2$ gels, gellan gum gels and hybrid gels based on gellan gum/LMWG. In all cases, the PG component is crosslinked using 0.15% wt/vol $CaCO_3$ and 1% wt/vol GdL. Loadings are given in % wt/vol. G' values are given in Pa. The G'/G'' crossover point refers to the % shear strain at which $G'' = G'$

LMWG load (%)	GG load (%)	Total load (%)	Gel trigger	G'	G'/G'' crossover (%)
0.4	—	0.4	Heat/cool	800	25.1
—	0.4	0.4	$CaCO_3$/GdL	1760	0.8
—	0.6	0.6	$CaCO_3$/GdL	4630	0.5
—	0.8	0.8	$CaCO_3$/GdL	8950	1.3
0.3	0.1	0.4	$CaCO_3$/GdL	2580	15.9
0.3	0.3	0.6	$CaCO_3$/GdL	11 300	7.4
0.3	0.5	0.8	$CaCO_3$/GdL	19 300	5.4

In terms of resistance to shear strain, the advantages of the hybrid hydrogel approach are once again evident. On its own, GG gels formed in this way are brittle, struggling to maintain integrity even at 1% shear strain. However, in the hybrid gels, this increases to at least 5%. The presence of the LMWG network significantly improves handleability of this gel, without impacting gel stiffness (indeed, stiffness is also enhanced).

To look in more detail at the effect of $CaCO_3$ concentration on the mechanical properties of the gels, we compared the elastic moduli of hybrid gels prepared using equal amounts of the two gelators (0.3% wt/vol), a fixed GdL concentration (1.0% wt/vol) and different $CaCO_3$ concentrations (0.075, 0.15 and 0.3% wt/vol). The G' of the gel prepared at the lowest cross-linker concentration (0.075% wt/vol) is 5720 Pa (Fig. S36, ESI†), which increased to 11 300 and 17 200 Pa (Fig. S37, ESI†) when the gels were prepared with 0.15% and 0.3% wt/vol of $CaCO_3$. This is consistent with a higher availability of Ca^{2+} ions to cross-link GG. To explore whether GdL concentration could also affect gel stiffness, we studied the gels using a fixed $CaCO_3$ concentration (0.15% wt/vol) and different amounts of GdL (0.8, 1.0 and 1.2% wt/vol). The gels prepared with 1.2% wt/vol GdL had the highest G' (14 300 Pa; Fig. S39, ESI†) compared to the gels prepared using 0.8% wt/vol (10 900 Pa; Fig. S38, ESI†). This reflects a higher percentage of $CaCO_3$ being converted into Ca^{2+} and H_2CO_3 with higher GdL concentrations. In summary, the rheological properties can easily tuned by controlling the starting conditions – valuable for application in regenerative medicine given the impact of gel stiffness on cell fate, adhesion, migration and differentiation.[24]

Photo-initiated and patterned gels based on DBS-$CONHNH_2$/GG cross-linked with $CaCO_3$/DPIN

We reasoned that by using diphenyliodonium nitrate (DPIN) as a photoacid generator instead of GdL, it may be possible to induce GG crosslinking under UV light. Although this approach has been used for the photoinduced gelation and patterning of calcium alginate,[25] we cannot find evidence of it having previously been applied to gellan gum.

To test the method, we first combined GG (0.4, 0.6, 0.8 and 1.3% wt/vol) with $CaCO_3$ (0.15% wt/vol) and the photo-acid generator diphenyliodonium nitrate (DPIN, 0.8% wt/vol) and exposed the mixture to a high intensity UV lamp for 2 h. After this time, self-supporting gels were obtained (Fig. S40, ESI†); thus confirming Ca^{2+} release and GG cross-linking could be triggered in this way. We applied this procedure to DBS-$CONHNH_2$/GG hybrid gels. DBS-$CONHNH_2$ (0.3% wt/vol) was dispersed in water and combined with $CaCO_3$ (0.15% wt/vol), DPIN (0.8% wt/vol) and GG (0.5% wt/vol). The mixture was heated until dissolution of the LMWG and then exposed to the UV light for 2 h to give self-supporting UV-activated gels (Fig. 1, 4a and Fig. S40, ESI†).

Photopatterning was achieved by applying a photomask on a pre-formed DBS-$CONHNH_2$ gel in a tray (5 cm × 5 cm), selectively triggering Ca^{2+} release only in the regions exposed to the UV light. This is a technique we have previously applied, and is an efficient method for photopatterning, as the pre-formed gel helps limit convection and diffusion, with the pH-responsive gelator only assembling in the regions exposed to the UV light.[14d,26] DBS-$CONHNH_2$/GG photo-patterned gels were prepared by combining DBS-$CONHNH_2$ (0.3% wt/vol) with $CaCO_3$ (0.15% wt/vol), DPIN (0.8% wt/vol) and GG (0.3% wt/vol). The mixture was heated until complete dissolution of the LMWG and transferred to the glass tray. The sample was left undisturbed for 15 min to allow assembly of the DBS-$CONHNH_2$ network. A laser-printed mask was placed on top of the glass tray and the gel exposed to UV light for 2 h. To avoid disruption of the gel due to heating effects, ice was placed below the glass tray. After photo-irradiation, the desired circular pattern formed by the cross-linked polymer was clearly visible within the DBS-$CONHNH_2$ gel (Fig. 4b).

TEM and SEM microscopy showed a self-assembled nanofibrillar network, similar to the hybrid gel prepared in sample vials using GdL (Fig. 4c, d and Fig. S41–S44, ESI†). The properties of the UV-triggered gels were studied in terms of thermal stability and rheology. Both gels had a T_{gel} of >100 °C, confirming that the presence of crosslinked GG improves the thermal stability of the LMWG (Table S6, ESI†). In terms of rheology, the photo-activated GG-only gel (0.6% wt/vol) has an elastic modulus of 8670 Pa (Table 3 and Table S7, Fig. S46, ESI†), higher than the G' of the corresponding gel prepared using GdL (G' = 4630 Pa). The hybrid gel prepared by photo-activation using an equal amount of each

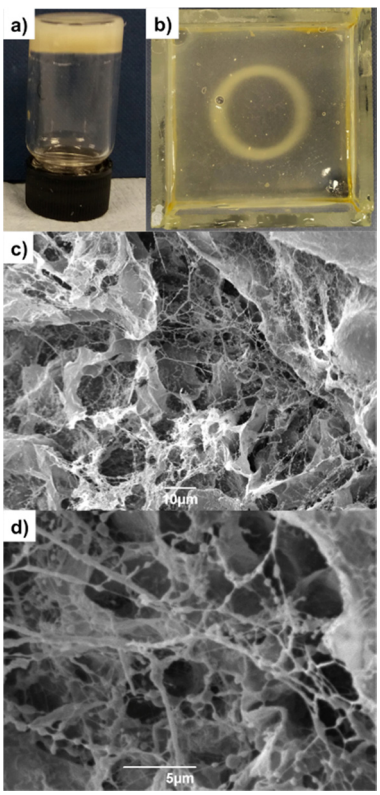

Fig. 4 (a) Photographic image of photoactivated DBS-$CONHNH_2$/GG hybrid gel cross-linked with $CaCO_3$/DPIN. (b) Photopatterned DBS-$CONHNH_2$/GG hybrid gel cross-linked with $CaCO_3$/DPIN. (c and d) SEM images of photoactivated DBS-$CONHNH_2$/GG hybrid gel.

Table 3 Rheological data as determined using oscillatory rheometry with a parallel plate geometry, for DBS-CONHNH$_2$ gels, gellan gum gels, alginate gels and hybrid gels based on gellan gum/LMWG and alginate/LMWG.[14d] In all cases, the PG component is crosslinked using 0.15% wt/vol $CaCO_3$ and 0.8% wt/vol DPIN. Loadings are given in % wt/vol. G' values are given in Pa. The G'/G'' crossover point refers to the % shear strain at which $G'' = G'$

LMWG load (%)	GG load (%)	Alginate load (%)	Total load (%)	Gelation trigger	G'	G'/G'' crossover (%)
0.4	—	—	0.4	Heat/cool	800	25.1
—	0.6		0.6	DPIN	8670	6.4
0.3	0.3		0.6	DPIN	12 486	8.0
		0.6	0.6	DPIN	32.5	79.3
0.3		0.3	0.6	DPIN	117	25.1

gelator (0.3% wt/vol) also had a slightly higher G' (12 486 Pa; (Table 3 and Fig. S45, ESI†) than the gel prepared with GdL (11 300 Pa). This indicates photoactivation is an effective technique for these gels. The hybrid hydrogel also shows a slightly higher resistance to shear strain than the GG-only system. These photoactivated GG-only and GG/LMWG hybrid gels are very much stiffer than the equivalent materials formed using calcium alginate (Table 3). This demonstrates that GG can yield much improved stiffness in photoactivated and photo-patterned hybrid hydrogels than alginate, which may offer significant advantages in tailored tissue engineering applications.[27]

Summary of rheological performance

In summary (Fig. 5), irrespective of the mode of gel triggering, the GG-only gels have high rheological stiffness, but poor stability to shear – particularly in contrast with alginate-only gels. These differences in gel mechanical properties can be attributed to intrinsic differences between the polymers (*e.g.* molecular weight, structure, conformation and crystallinity).[28] Forming hybrid gels between GG and DBS-CONHNH$_2$ further enhances the stiffness (Fig. 5A) because there are now two interwoven networks and also perhaps partly because GG gelation is also induced by temperature and it therefore may benefit from annealing in the two-component system. In all cases, the hybrid gels also have significantly increased resistance to shear strain (Fig. 5B), as the hybrid gels take on some of the increased resistance to shear of the LMWG system.

In this way, applying the hybrid gel approach to GG significantly enhances its rheological performance. In comparison with hybrid gels based on calcium alginate (Fig. 5C), the stiffnesses are significantly higher and would be more similar to those required for bone tissue engineering.[17,24] Hence there are benefits to having changed PG in terms of optimising this rheological characteristic.

In situ formation of AgNPs

We then wanted to demonstrate that the LMWG retained its unique chemical characteristics within these hybrid gels. In particular, we decided to induce the *in situ* formation of AgNPs, exploiting the unique reducing power of the DBS-CONHNH$_2$ LMWG that converts Ag(I) to Ag(0) when exposed

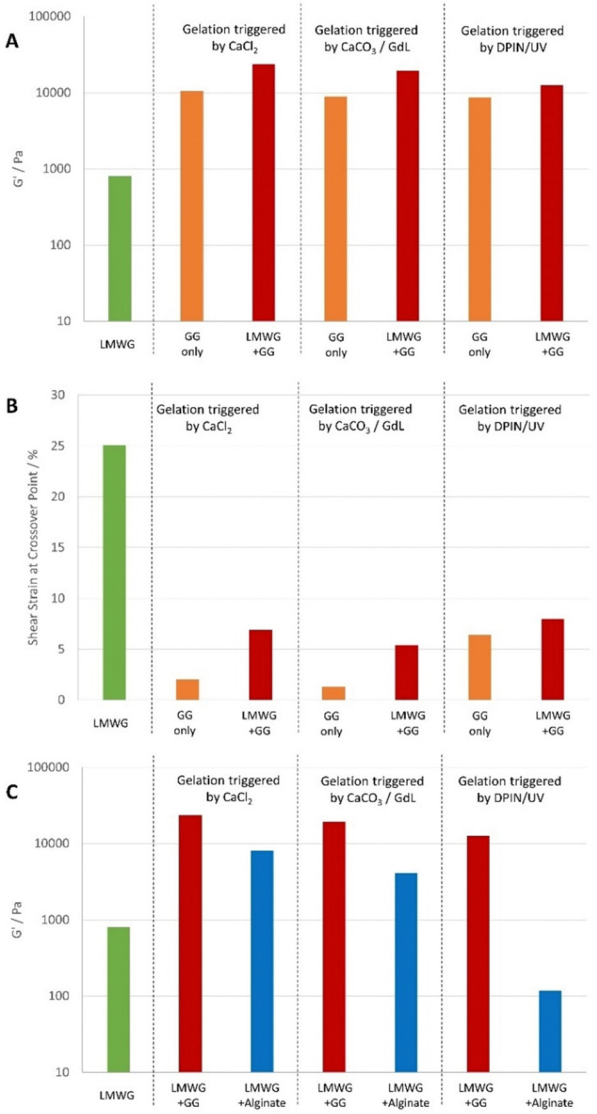

Fig. 5 Summary of rheological performance of the hybrid gels. (A) Hybrid GG/LMWG gels (red bars) show enhanced stiffness over GG-only gels (orange bars). (B) Hybrid GG/LMWG gels (red bars) show greater resistance to shear strain than GG-only gels (orange gels), that fracture very easily. (C) Hybrid GG/LMWG gels (red bars) have greater stiffness than equivalent alginate/LMWG hybrid hydrogels (blue bars). In each case, LMWG is 0.3% wt/vol. For $CaCl_2$ and $CaCO_3$/GdL triggered gels, total gelator loading is 0.8% wt/vol, hybrid gels are 0.3% wt/vol LMWG and 0.5% wt/vol GG or alginate. For $CaCO_3$/DPIN/UV triggered gels, the total gelator loading is 0.6% wt/vol, hybrid gels are 0.3% wt/vol LMWG and 0.3% wt/vol GG or alginate.

to silver salt solutions. It is well-known that precious metal nanoparticles (NPs) can promote osteogenesis,[29] and we reasoned that in the longer term, it would be useful to incorporate them in these stiff hybrid gels, which have suitable rheological properties for this type of application.[17] We previously studied *in situ* formation of AgNPs in DBS-CONHNH$_2$/alginate gel beads.[14d,15b]

DBS-CONHNH$_2$/GG gel beads were prepared by combining DBS-CONHNH$_2$ (0.3% wt/vol) with GG (0.3% wt/vol), GdL

(1.0% wt/vol) and $CaCO_3$ (0.15% wt/vol) and compared to DBS-$CONHNH_2$/GG gels prepared in sample vials. To remove residual ions, the beads were washed multiple times with water. AgNP formation was then induced by exposing the gels to a solution of $AgNO_3$ (10 mM, 1 or 3 mL) for 72 h. The formation of the AgNPs was confirmed by the intense colour change of the gels (from white to orange; Fig. 6a) and by TEM, which clearly showed the presence of NPs dispersed between gel fibres with an average diameter <40 nm (Fig. 6b, c, g and Fig. S49, ESI†), similar to those formed in the DBS-$CONHNH_2$ gel (Fig. 6g and Fig. S48, ESI†). Some sort of AgNPs were also formed in GG-only gels (Fig. 6d–g and Fig. S50, ESI†), however these gels did not undergo the intense colour change, and the NPs were not uniformly distributed, showing very variable sizes and much larger aggregates (Fig. 6g).

The maximum amount of Ag(I) incorporated into the gel beads was quantified by precipitation titration of NaCl, in the presence of K_2CrO_4 as an indicator. Each hybrid gel bead (20 μL volume) incorporated *ca.* 0.3 μmol of Ag(I), corresponding to *ca.* 13 μmol of Ag(I)/mL of gel (Table S8, ESI†). Each mL of gel can contain up to 6.32 μmol of gelator, clearly indicating *ca.* 2 : 1 Ag : DBS-$CONHNH_2$ stoichiometry. This is consistent with a model in which the acylhydrazide groups (two per gelator) are intimately involved in reducing Ag(I) to Ag(0).[15] This result is very similar to Ag(I) uptake in the DBS-$CONHNH_2$ gels (16.7 μmol of Ag(I)/mL of gel; Table S8, ESI†), thus confirming the LMWG maintains its function within the hybrid gel beads. Ag(I) release from the gels was also investigated, with *ca.* 20% of the loaded Ag being rapidly released (<30 min) in the form of Ag(I) (Fig. S47, ESI†), while the remainder remains in place in the form of AgNPs. It is clear that any residual excess Ag(I) is therefore easily and rapidly removed, avoiding any problems with its potential cytotoxicity[30] in our stem cell growth experiments (see below).

The mechanical properties of the AgNP-loaded hybrid gels prepared in sample vials (0.3% DBS-$CONHNH_2$, 0.3% alginate, 0.15% $CaCO_3$ and 1.0% GdL) were also studied by oscillatory rheology. Overall, the hybrid gels loaded with AgNPs (10 μmol mL^{-1} of gel) had similar elastic moduli (G' = 11 700 Pa, Table S11 and Fig. S53, ESI†) to the unloaded gels (G' = 11 300 Pa). However, if the AgNP loading was increased to very high level (30 μmol mL^{-1} of gel), the elastic modulus fell somewhat (G' = 4950 Pa; Table S11 and Fig. S54, ESI†). Similar trends were also observed for the corresponding DBS-$CONHNH_2$ (Table S11 and Fig. S51–S52, ESI†) and gellan gum gels (Table S11 and Fig. S55, S56, ESI†) and it is probably due to disruption of the interactions between fibres within the gel network at very high AgNP loadings.

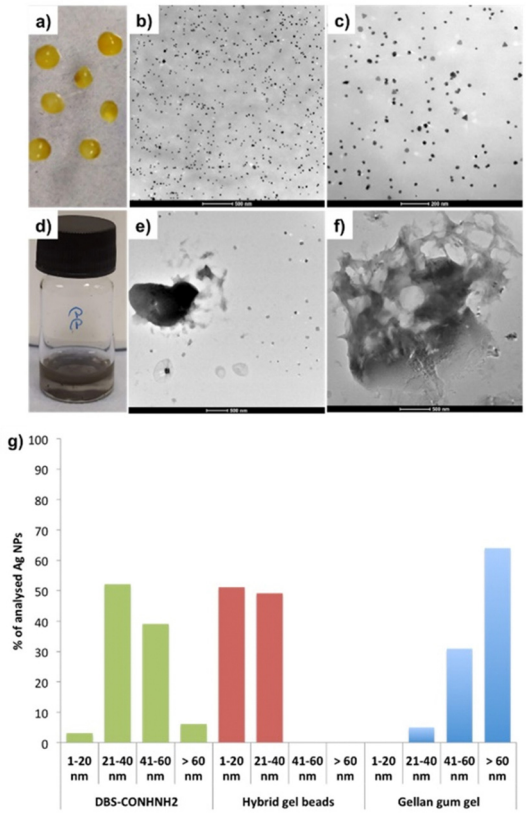

Fig. 6 (a–c) Photographic and TEM images of DBS-$CONHNH_2$/GG hybrid gel beads loaded with Ag NPs. (d–f) Photographic and TEM images of GG gels loaded with Ag NPs. (g) Graph of Ag NPs size distribution in DBS-$CONHNH_2$ bulk gel (green), DBS-$CONHNH_2$/GG hybrid gel beads (red) and gellan gum gel (blue).

Stem cell growth

We then explored if the DBS-$CONHNH_2$/GG hybrid gel beads could support stem cell growth. Preliminary cytotoxicity and viability experiments were performed on a human mesenchymal stem cell line (Y201)[31] using different AgNP loadings. The gels were prepared in a 48-well plate and loaded with 0.0125 or 10.0 μmol of $AgNO_3$/mL of gel (low loading and high loading respectively). The samples were transferred to the middle of a 6-well plate, where the cells were seeded. Due to their fragility, gels based only on DBS-$CONHNH_2$ could not be transferred; therefore, these gels were prepared directly on the 6-well plates using bottomless vials, which did not allow loading the gels with $AgNO_3$. After 48 h, the gels without AgNPs and those incorporating a low 0.0125 μmol loading of $AgNO_3$/mL of gel showed normal cell growth and did not exhibit any 'zone of inhibition' (Fig. S57 and S58, ESI†) – as such, they were considered to be non-toxic. However, the gels incorporating a high Ag loading (10.0 μmol of $AgNO_3$/mL of gel), showed a rather large zone of inhibition around them (2.90–3.60 mm; Fig. S58, ESI†) and must therefore be considered toxic to stem cells. This is in-line with previous studies showing high concentrations of Ag^+ ions can affect mammalian cell survival.[32]

To obtain more detailed data on biocompatibility, we performed an Alamar Blue assay on Y201 cells grown on gels with different AgNP loadings and control gels without AgNPs. DBS-$CONHNH_2$ and GG gels were prepared directly on 96 well plates, whereas the hybrid gel beads were prepared and then transferred to the 96 well plates. To ensure the cells were adhering to the gels rather than the plate surface, we used non-adherent plates. The gels were loaded with different $AgNO_3$ loadings (0.00625, 0.0125, 0.05, 0.1, 1.0 and 10 μmol of $AgNO_3$/mL of gel) and cell metabolic activity was monitored over 10 days (day 0, 3, 6 and 10).

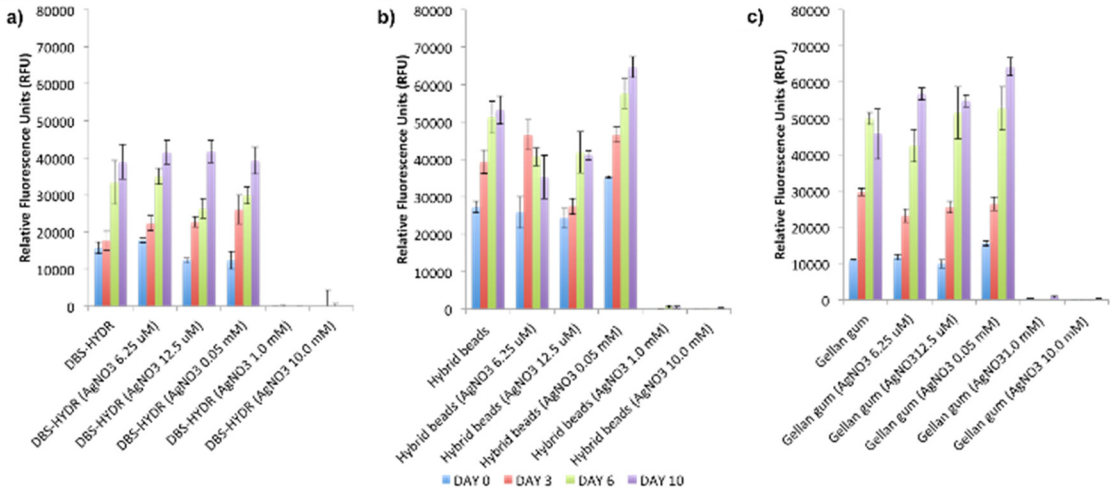

Fig. 7 Alamar blue assay results at day 0, 3, 6 and 10 for gels loaded with different $AgNO_3$ concentrations (N = 6, mean reported, error bars represent standard error, DBS-HYDR = DBS-$CONHNH_2$).

Pleasingly, the obtained results showed the cells were metabolically active in the gels without AgNPs and in those loaded with 0.00625–0.1 μmol of $AgNO_3$/mL of gel (Fig. 7). Higher $AgNO_3$ loadings (1.0 and 10 μmol of $AgNO_3$/mL of gel) were, as expected, toxic across the different gel types tested (Fig. 7) in agreement with the preliminary study described above. Compared to the DBS-$CONHNH_2$ gels, the gel beads showed higher fluorescence values over the ten days, indicative of higher cell metabolic activity, which can be related to a higher number of cells. This is probably due to the higher surface area of the gel beads available for cell anchorage and penetration inside the gels. For the GG-only gels, cell growth was initially slower than on the hybrid gel beads, which may reflect enhanced initial cell anchorage induced by the LMWG, although by day 6 the GG-only beads were equivalent to the LMWG/GG hybrids. In each case, cell growth was similar in the presence and absence of AgNPs.

To verify if the gels could support cell growth over a longer period of time, a viability test was performed over 21 days (day 0, 7, 14 and 21) on the gels loaded with lower $AgNO_3$ loadings (0.00625 and 0.0125 μmol of $AgNO_3$/mL of gel; Fig. S59, ESI†) and control gels without AgNPs. Pleasingly, the results showed that the cells had good metabolic activity in all of the tested gels for the whole duration of the study. These preliminary biocompatibility tests demonstrate that the DBS-$CONHNH_2$/GG hybrid gel beads (with or without AgNPs) support the growth of human mesenchymal stem cells over time and could potentially be used in tissue engineering.

Gels incorporating AgNPs have previously been demonstrated to induce osteogenesis in mesenchymal stem cells and bone tissue repair.[29] Our gels could therefore be promising in this setting, particularly given the stiffness of the GG gels. Specifically, our AgNP-loaded shapeable biomaterials may be effective bone fillers to facilitate bone regeneration whilst preventing infections.[33] Indeed, AgNPs are well-known to have antibacterial activity.[14d,34] Future studies will explore cell function and osteogenic activity of cells grown on our AgNP gel beads as well as antimicrobial properties.

Conclusion

To conclude we have demonstrated that gellan gum can be used as a polymer gel to obtain DBS-$CONHNH_2$/GG hybrid gels. Gel assembly can be achieved using a variety of different triggers. Exposure of pre-formed LMWG beads loaded with GG to a bath of $CaCl_2$ induces rapid GG crosslinking from the outside inwards. Conversely, loading the beads with GG, insoluble $CaCO_3$ and acid-generating GdL led to hybrid gel beads *via* an internal slow acidification gelation. By substituting GdL with the photoacid generator DPIN to induce GG crosslinking, this process could be activated by UV light exposure. Performing this process with a photo-mask made it possible to fabricate photopatterned gels with different compositions in the different domains.

The gels obtained using these different triggering methods were fully characterised by a range of techniques. Importantly, in all cases, the hybrid gels were even stiffer than those formed by GG alone, as a result of the interpenetrating LMWG and PG networks. The hybrid DBS-$CONHNH_2$/GG gels are also significantly stiffer than equivalent hybrid hydrogels previously made with calcium alginate as the PG.[14a,d] Furthermore, the enhanced stiffness does not come at the cost of additional sensitivity to shear strain – indeed, the hybrid gels are considerably more stable to shear strain than the GG-only gels. In summary, the presence of the LMWG enhances both the stiffness and shear strain stability of gellan gum.

To confirm the DBS-$CONHNH_2$ kept its unique chemical function when combined with GG, we induced *in situ* AgNP formation and demonstrated this required the presence of the LMWG. Finally, biological tests were performed on human mesenchymal stem cells allowed us to identify non-toxic AgNP loadings and demonstrated that the cells can thrive in the hybrid gel beads for long periods of time (*i.e.* at least 21 days). We suggest that our shaped DBS-$CONHNH_2$/GG gels are promising materials for orthopaedic applications. Further studies to exploit this are currently being carried out in our laboratories.

Author contributions

Funding was obtained by D. K. S. who developed the overarching LMWG shaping and patterning concept. C. C. P. conceptualised the use of gellan gum in this application and carried out all of the experimental work with supervisory guidance and input from P. G. G. (biological studies) and D. K. S. (materials chemistry). C. C. P. and D. K. S. wrote the manuscript with input from P. G. G.

Conflicts of interest

There are no conflicts to declare.

Acknowledgements

We thank EPSRC (EP/P03361X/1) and EPSRC IAA (University of York) for funding. Karen Hodgkinson (Bioscience Technology Facility, Department of Biology, University of York) is acknowledged for optical microscopy, TEM and SEM imaging.

Notes and references

1 (*a*) A. R. Hirst, B. Escuder, J. F. Miravet and D. K. Smith, *Angew. Chem., Int. Ed.*, 2008, **47**, 8002–8018; (*b*) J. Zhou, J. Li, X. Du and B. Xu, *Biomaterials*, 2017, **129**, 1–27; (*c*) J. Hoque, N. Sangaj and S. Varghese, *Macromol. Biosci.*, 2019, **19**, e1800259; (*d*) J. Mayr, C. Saldías and D. Díaz Díaz, *Chem. Soc. Rev.*, 2018, **47**, 1484–1515; (*e*) D. K. Smith in *Molecular Gels: Structure and Dynamics*, ed. R. G. Weiss, Royal Society of Chemistry, Cambridge, 2018, pp. 300–371.

2 (*a*) *Polymer Gels: Fundamentals and Applications*, ed. H. B. Bohidar, P. Dubin and Y. Osada, American Chemical Society, Washington DC, 2002; (*b*) B. V. Slaughter, S. S. Khurshid, O. Z. Fisher, A. Khademhosseini and N. A. Peppas, *Adv. Mater.*, 2009, **21**, 3307–3329; (*c*) J. Li and D. J. Mooney, *Nat. Rev. Mater.*, 2016, **1**, 16071.

3 (*a*) R. G. Weiss, *J. Am. Chem. Soc.*, 2014, **136**, 7519–7530; (*b*) X. Du, J. Zhou, J. Shi and B. Xu, *Chem. Rev.*, 2015, **115**, 13165–13307; (*c*) E. R. Draper and D. J. Adams, *Chem*, 2017, **3**, 390–410.

4 For reviews see: (*a*) D. J. Cornwell and D. K. Smith, *Mater. Horiz.*, 2015, **2**, 279–293; (*b*) L. C. Li, R. Q. Sun and R. L. Zheng, *Mater. Des.*, 2021, **197**, 109209. For selected examples: (*c*) J. Wang, Z. Wang, J. Gao, L. Wang, Z. Yang, D. Kong and Z. Yang, *J. Mater. Chem.*, 2009, **19**, 7892–7896; (*d*) R. Huang, W. Qi, L. Feng, R. Su and Z. He, *Soft Matter*, 2011, **7**, 6222–6230; (*e*) P. Li, X.-Q. Dou, C.-L. Feng and D. Zhang, *Soft Matter*, 2013, **9**, 3750–3757; (*f*) D. J. Cornwell, B. O. Okesola and D. K. Smith, *Soft Matter*, 2013, **9**, 8730–8736; (*g*) J. Chen, N. Tao, S. Fang, Z. Chen, L. Liang, X. Sun, J. Li and Y.-N. Liu, *New J. Chem.*, 2018, **42**, 9651–9657; (*h*) B. C. Baker, I. German, G. C. Stevens, H. M. Colquhoun and W. Hayes, *RSC Adv.*, 2018, **8**, 41445; (*i*) B. P. Nowak and B. J. Ravoo, *Soft Matter*, 2020, **16**, 7299–7304; (*j*) H. Shigemitsu, R. Kubota, K. Nakamura, T. Matsuzaki, S. Minami, T. Aoyama, K. Urayama and I. Hamachi, *Nat. Commun.*, 2020, **11**, 3859.

5 (*a*) P. R. A. Chivers and D. K. Smith, *Nat. Rev. Mater.*, 2019, **4**, 463–478; (*b*) G. A. Primo and A. Mata, *Adv. Funct. Mater.*, 2021, **31**, 2009574.

6 (*a*) I. Giavasis, L. M. Harvey and B. McNeil, *Crit. Rev. Biotechnol.*, 2000, **20**, 177–211; (*b*) I. B. Bajaj, S. A. Survase, P. S. Saudagar and R. S. Singhal, *Food Technol. Biotechnol.*, 2007, **45**, 341–354; (*c*) A. M. Fialho, L. M. Moreira, A. T. Granja, A. O. Popescu, K. Hoffmann and I. Sa-Correia, *Appl. Microbiol. Biotechnol.*, 2008, **79**, 889–900; (*d*) E. R. Morris, K. Nishinari and M. Rinaudo, *Food Hydrocoll.*, 2012, **28**, 373–411; (*e*) V. D. Prajapati, G. K. Jani, B. S. Zala and T. A. Khutliwala, *Carbohydr. Polym.*, 2013, **93**, 670–678.

7 D. E. Pszczola, *Food Technol.*, 1993, **47**, 94–96.

8 (*a*) G. R. Sanderson and R. C. Clark, *Food Technol.*, 1983, **37**, 63–70; (*b*) N. E. Wedamulla and W. A. J. P. Wijesinghe, *Trends Carbohydr. Res.*, 2021, **13**, 35–49.

9 L. R. Stevens, K. J. Gilmore, G. G. Wallace and M. I. H. Panhuis, *Biomaterials*, 2016, **4**, 1276–1290.

10 A. P. Chiriac, A. Ghilan, I. Neamtu, L. E. Nita, A. G. Rusu and V. M. Chiriac, *Macromol. Biosci.*, 2019, **19**, 1900187.

11 (*a*) T. Osmalek, A. Froelich and S. Tasarek, *Int. J. Pharm.*, 2014, **466**, 328–340; (*b*) F. S. Palumbo, S. Federico, G. Pitarresi, C. Fiorica and G. Giammona, *Carbohydr. Polym.*, 2019, **229**, 115430; (*c*) C. Villarreal-Otalvaro and J. M. Coburn, *ACS Biomater. Sci. Eng.*, 2022, DOI: **10.1021/acsbiomaterials.1c00685**.

12 T. Muthukumar, J. E. Song and G. Khang, *Molecules*, 2020, **24**, 4514.

13 (*a*) A. H. Bacelar, J. Silva-Correia, J. M. Oliveira and R. L. Reis, *J. Mater. Chem. B*, 2016, **4**, 6164–6174; (*b*) K. M. Zia, S. Tabasum, M. F. Khan, N. Akram, N. Akhter, A. Noreen and M. Zuber, *Int. J. Biol. Macromol.*, 2018, **109**, 1068–1087.

14 (*a*) C. C. Piras, P. Slavik and D. K. Smith, *Angew. Chem., Int. Ed.*, 2020, **59**, 853–859; (*b*) C. C. Piras, A. G. Kay, P. G. Genever and D. K. Smith, *Chem. Sci.*, 2021, **12**, 3958–3965; (*c*) C. C. Piras, A. K. Patterson and D. K. Smith, *Chem. – Eur. J.*, 2021, **27**, 13203–13210; (*d*) C. C. Piras, C. S. Mahon, P. G. Genever and D. K. Smith, *ACS Biomater. Sci Eng.*, 2022, **8**, 1829–1840; (*e*) C. C. Piras and D. K. Smith, *Chem. – Eur. J.*, 2021, **27**, 14527–14534.

15 (*a*) B. O. Okesola, S. K. Suravaram, A. Parkin and D. K. Smith, *Angew. Chem., Int. Ed.*, 2016, **55**, 183–187; (*b*) C. C. Piras, C. S. Mahon and D. K. Smith, *Chem. – Eur. J.*, 2020, **26**, 8452–8457.

16 (*a*) B. O. Okesola and D. K. Smith, *Chem. Commun.*, 2013, **49**, 11164–11166; (*b*) P. R. A. Chivers, J. A. Kelly, M. J. S. Hill and D. K. Smith, *React. Chem. Eng.*, 2020, **5**, 1112–1117.

17 (*a*) Y. S. Pek, A. C. A. Wan, A. Shekaran, L. Zhuo and J. Y. Ying, *Nat. Nanotechnol.*, 2008, **3**, 671–675; (*b*) R. G. M. Breuls, T. U. Jiya and T. H. Smit, *Open Orthop. J.*, 2008, **2**, 103–109; (*c*) V. Pandit, J. M. Zuidema, K. N. Venuto, J. Macione, G. Dai, R. J. Gilbert and S. P. Kotha, *Tissue Eng. Part A*, 2013, **19**, 2452–2463; (*d*) Y. Hu, W. Gao, F. Wu, H. Wu, B. He and J. He, *J. Mater. Chem. B*, 2016, **4**,

3504–3508; (*e*) E. V. Alakpa, V. Jayawarna, A. Lampel, K. V. Burgess, C. C. West, S. C. J. Bakker, S. Roy, N. Javid, S. Fleming, D. A. Lamprou, J. Yang, A. Miller, A. J. Urquhart, P. W. J. M. Frederix, N. T. Hunt, B. Péault, R. V. Ulijn and M. J. Dalby, *Chem*, 2016, **1**, 298–319; (*f*) B. Yi, Q. Xu and W. Liu, *Bioactive Mater.*, 2022, **15**, 82–102.

18 P. Gurikov and I. Smirnova, *Gels*, 2018, **4**, 14.

19 Y. Pocker and E. Green, *J. Am. Chem. Soc.*, 1973, **95**, 113–119.

20 For selected examples see: (*a*) C. K. Kuo and P. X. Ma, *Biomaterials*, 2001, **22**, 511–521; (*b*) C. K. Kuo and P. X. Ma, *J. Biomed. Mater.*, 2008, **84A**, 899–907; (*c*) A. Schmitt, P. Rödel, C. Anamur, C. Seeliger, A. B. Imhoff, E. Herbst, S. Vogt, M. van Griensven, G. Winter and J. Engert, *PLOS One*, 2015, **10**, e0118937; (*d*) Z. Li, A. K. Pearce, A. P. Dove and R. K. O'Reilly, *Polymers*, 2021, **13**, 2202; (*e*) L. Sardelli, M. Tinesi, F. Briatico-Vangosa and P. Petrini, *Soft Matter*, 2021, **17**, 8105–8117.

21 A. Li, T. Gong, X. Yang and Y. R. Guo, *Int. J. Biol. Macromol.*, 2020, **151**, 257–267.

22 (*a*) T. E. L. Douglas, W. Piwowarczyk, E. Pamula, J. Liskova, D. Schaubroeck, S. C. G. Leeuwenburgh, G. Brackman, L. Balcauen, R. Detsch, H. Declercq, K. Cholewa-Kowalska, A. Dokupil, V. M. J. I. Cuijpers, F. Vanhaecke, R. Cornelissen, T. Coenye, A. R. Boccaccini and P. Dubruel, *Biomed. Mater.*, 2014, **9**, 045014; (*b*) T. E. L. Douglas, A. Lapa, K. Reczynska, M. Krok-Borkowicz, K. Pietryga, S. K. Samal, H. A. Declercq, D. Schaubroeck, M. Boone and P. van der Voort, *Biomed. Mater.*, 2016, **11**, 065011.

23 A. Li, T. Gong, X. Li, X. Li, X. Yang and Y. Guo, *Int. J. Biol. Macromol.*, 2020, **156**, 565–575.

24 (*a*) M. Ahearne, *Interface Focus*, 2014, **4**, 20130038; (*b*) Y.-H. Tsou, J. Khoneisser, P.-C. Huang and X. Xu, *Bioactive Mater.*, 2016, **1**, 39–55; (*c*) S.-B. Han, J.-K. Kim, G. Lee and D.-H. Kim, *Adv. Biosyst.*, 2020, **4**, 2000247; (*d*) S. Yin and Y. Cao, *Acta Biomater.*, 2021, **128**, 1–20; (*e*) L. Tianyi, T. Bowen, Z. Lengjing, W. Yating and L. Jinfeng, *Front. Bioeng. Biotechnol.*, 2022, **10**, 817391.

25 (*a*) V. Javvaji, A. G. Baradwaj, G. F. Payne and S. R. Raghavan, *Langmuir*, 2011, **27**, 12591–12596; (*b*) L. Liu, F. Wu, X.-J. Ju, R. Xie, W. Wang, C. H. Niu and L.-Y. Chu, *J. Colloid Interface Sci.*, 2013, **404**, 85–90; (*c*) A. K. Higham, C. A. Bonino, S. R. Raghavan and S. A. Khan, *Soft Matter*, 2014, **10**, 4990–5002; (*d*) H. Oh, A. X. Lu, V. Javvaji, D. L. DeVoe and S. R. Raghavan, *ACS Appl. Mater. Interfaces*, 2016, **8**, 17529–17538; (*e*) T. M. Valentin, S. E. Leggett, P.-Y. Chen, J. K. Sodhi, L. H. Stephens, H. D. McClintock, J. Y. Sim and I. Y. Wong, *Lab Chip*, 2017, **17**, 3474–3488.

26 (*a*) D. J. Cornwell, B. O. Okesola and D. K. Smith, *Angew. Chem., Int. Ed.*, 2014, **53**, 12461–12465; (*b*) D. J. Cornwell, O. J. Daubney and D. K. Smith, *J. Am. Chem. Soc.*, 2015, **137**, 15486–15492; (*c*) C. C. Piras and D. K. Smith, *Chem. – Eur. J.*, 2018, **25**, 11318–11326; (*d*) D. J. Cornwell and D. K. Smith, *Chem. Commun.*, 2020, **56**, 7029–7032.

27 (*a*) M. Guvendiren and J. A. Burdick, *Curr. Opin. Biotechnol.*, 2013, **24**, 841–846; (*b*) A. Gelmi and C. E. Schutt, *Adv. Healthcare Mater.*, 2020, **10**, 2001125; (*c*) D. K. A. Kanioura, M. Chatzichristidi, K. G. Beltsios, S. E. Kakabakos and P. S. Petrou, *Eur. Polym. J.*, 2022, **162**, 110896.

28 (*a*) E. Miyoshi, T. Takaya and K. Nishinari, *Carbohydr. Polym.*, 1996, **30**, 109–119; (*b*) M. Jaspers, M. Dennison, M. F. J. Mabesoone, F. C. MacKintosh, A. E. Rowan and P. H. J. Kouwer, *Nat. Commun.*, 2014, **5**, 5808; (*c*) A. Li, T. Gong, X. Li, X. Li, X. Yang and Y. Guo, *Int. J. Biol. Macromol.*, 2020, **156**, 565–575; (*d*) D. Ji and J. Kim, *Adv. NanoBiomed. Res.*, 2021, **1**, 2100026.

29 (*a*) X. Liu, W. He, Z. Fang, A. Kienzle and Q. Feng, *J. Biomed. Nanotechnol.*, 2014, **10**, 1277–1285; (*b*) H. Qin, C. Zhu, Z. An, Y. Jiang, Y. Zhao, J. Wang, X. Liu, B. Hui, X. Zhang and Y. Wang, *Int. J. Nanomed.*, 2014, **9**, 2469–2478; (*c*) A. K. Nguyen, R. Patel, J. M. Noble, J. Zheng, R. J. Narayan, G. Kumar and P. L. Goering, *Appl. Vitro Toxicol.*, 2019, **5**, 123–133; (*d*) H. Xie, P. Wang and J. Wu, *Artif. Cells Nanomed. Biotechnol.*, 2019, **47**, 260–267.

30 (*a*) L. Kvitek, A. Panacek, R. Prucek, J. Soukupova, M. Vanickova, M. Kolar and R. Zboril, *J. Phys.: Conf. Ser.*, 2011, **304**, 012029; (*b*) C. Liao, Y. Li and S. C. Tjong, *Int. J. Mol. Sci.*, 2019, **20**, 449.

31 S. James, J. Fox, F. Afsari, J. Lee, S. Clough, C. Knight, J. Ashmore, P. Ashton, O. Preham, M. Hoogduijn, R. D. R. Ponzoni, Y. Hancock, M. Coles and P. Genever, *Stem Cell Rep.*, 2015, **4**, 1004–1015.

32 (*a*) L. Kvitek, A. Panacek, R. Prucek, J. Soukupova, M. Vanickova, M. Kolar and R. Zboril, *J. Phys.: Conf. Ser.*, 2011, **304**, 012029; (*b*) C. Liao, Y. Li and S. C. Tjong, *Int. J. Mol. Sci.*, 2019, **20**, 449.

33 (*a*) S. A. Brennan, C. N. Fhoghlú, B. M. DeVitt, F. J. O'Mahony, D. Brabazon and A. Walsh, *Bone Joint J.*, 2015, **97-B**, 582–589; (*b*) L.-L. Li, H.-W. An, B. Peng, R. Zheng and H. Wang, *Mater. Horiz.*, 2019, **6**, 1794–1811; (*c*) D. Burak, B. O. Okesola, D. W. Barrett, M. D'Este, T. T. Chowdhury, D. Eglin and A. Mata, *Acta Biomater.*, 2020, **109**, 82–94; (*d*) B. O. Okesola, S. Ni, B. Derkus, C. C. Galeano, A. Hasan, Y. Wu, J. Ramis, L. Buttery, J. I. Dawson, M. D'Este, R. O. C. Oreffo, D. Eglin, H. Sun and A. Mata, *Adv. Funct. Mater.*, 2020, **30**, 1906205; (*e*) B.-D. Zheng, J. Ye, Y.-C. Yang, Y.-Y. Huang and M.-T. Xiao, *Carbohydr. Polym.*, 2021, **275**, 118770.

34 (*a*) N. Durán, M. Durán, M. B. de Jesus, A. B. Seabra, W. J. Fávaro and G. Nakazato, *Nanomed.: Nanotechnol. Biol. Med.*, 2016, **12**, 789–799; (*b*) M. Bilal, T. Rasheed, H. M. N. Iqbal, H. Hu and X. Zhang, *Int. J. Pharmacol.*, 2017, **13**, 832–845; (*c*) A.-C. Burdusel, O. Gherasim, A. M. Grumezescu, L. Mogoanta, A. Ficai and E. Andronescu, *Nanomaterials*, 2018, **8**, 681; (*d*) F. Paladini and M. Pollini, *Materials*, 2019, **12**, 2540; (*e*) C. Liao, Y. Li and S. C. Tjong, *Int. J. Mol. Sci.*, 2019, **20**, 449.